PROCEEDINGS OF SPIE

A nine-channeled partial Mueller matrix polarimeter

Andrey Alenin, Israel Vaughn, J Scott Tyo

SPIE.

A nine-channeled partial Mueller matrix polarimeter

Andrey S. Alenin[a], Israel J. Vaughn[a], J. Scott Tyo[a]

[a]School of Engineering and IT, University of New South Wales Canberra, Canberra 2610 ACT, Australia.

ABSTRACT

We have recently introduced channeled-partial Mueller matrix polarimeters as a potential design for measuring a limited number of Mueller elements for remote sensing discrimination. Because in such systems the polarization information is modulated in space or spectrum, the corresponding carrier domain ends up sharing two different types of information, thus leading to a reduction of bandwidth for each. In this work, we concentrate on an efficient nine-channel/nine-reconstructables design, which limits the associated resolution loss by limiting the overall complexity of the system. Employing structured decomposition techniques allows us to produce a system description that provides an analytically deducible set of reconstructables that include m_{00}, any two linear combinations of the elements within the diattenuation vector, any two linear combinations of the elements within the polarizance vector, as well as the linear combinations specified by the Kronecker product of the diattenuation and polarizance vectors. Finally, we optimize the available polarimeter parameters to align the nine reconstructables with the desirables derived from sample data, while maintaining the ability to discriminate between different objects.

Keywords: Polarimetry, Polarization, Partial Mueller Matrix, Optimization

1. INTRODUCTION

Channeled polarimeters are a relatively recent,[1–7] but a powerful class of polarimeters.[8–11] They are esteemed for their inherent disposition towards constructing single-snapshot systems, whereby any additional polarization-sensitivity-induced temporal bandwidth limitations are eliminated at the expense of introducing such limitations in different domains, namely, space and/or spectrum. These bandwidth constraints come about as a consequence of modulations that are introduced within the respective domains: for whichever domains polarization information is modulated in, there is an associated loss of resolution in those same domains. This is because you are effectively sharing the total bandwidth of a domain between two different types of information: the native domain content, as well as the polarization content. Moreover, each new modulation carrier is not free either from the system cost perspective, or the noise performance side of things. In order to have enough diversified information within each channel for the Mueller matrix to be reconstructable, we need multiple modulations. And for the same reason that a Poincaré sphere requires two angles to navigate it, we need at least two modulations within both the Polarization State Generator (PSG) and the Polarization State Analyzer for them to be full-Stokes, and the polarimeter as a whole to be full-Mueller. Each of those subsequent modulation carriers reduces the signal amplitude by a factor of two, while multiple carries of different frequencies can produce channels that either combine or annihilate, which produces non-trivial information mixtures within each channel. Our original works tackled the unmixing performance optimization and offered ways to describe systems in a way that elucidates the channel contents and the conditioning of the implied inversion process. In this paper, we will discuss one system from a more recent development where we have introduced channeled partial Mueller matrix polarimeters (c-pMMPs). In that work, we looked to set out to adapt some of the partial polarimetry principles to channeled systems to minimize the number of channels produced and also to minimize the amount of sharing that occurred between polarization and spectrum information. This nine channeled partial Mueller matrix polarimeter (9-c-pMMP) fell out as a bit of a surprise—a few of the systems on the pareto-surface of the optimization had two of the carrier frequencies set to zero, which equivalently removed the corresponding elements altogether. Upon investigating that finding a bit closer, we realized that the 9-c-pMMP is an extremely efficient design from the perspective of having nine channels and nine reconstructables. Furthermore, it may represent a potential solution to alleviate the constraints associated with bandwidth-sharing by having fewer modulation-inducing elements, fewer carriers, and thus higher bandwidth. Figure 1 demonstrates this motivation.

Andrey S. Alenin: andrey.s.alenin@gmail.com

(a) 0 modulations   (b) 1 modulations (1 in y)   (c) 2 modulations (2 in y)   (d) 3 modulations (2 in y, 1 in x)   (e) 4 modulations (2 in y, 2 in x)   (f) 2 modulations (1 in y, 1 in x)
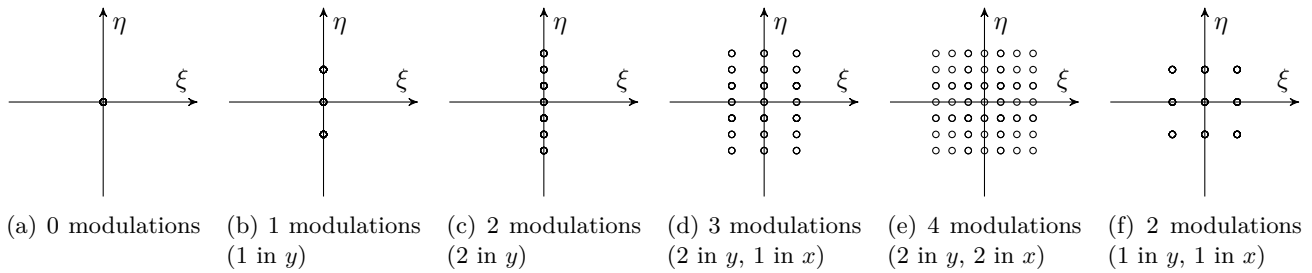
Figure 1: Subfigures (a)–(e) show how the channels split as more modulations are added. With each split, the bandwidth available to the channels within the new channel structure is reduced. Subfigure (f) is one of the 9-c-pMMP: the number of modulations is reduced to increase bandwidth.

In prior work, we looked at partial Mueller matrix polarimeters[12] (pMMPs) and c-pMMPs.[13] In both works, we used the data from Hoover and Tyo[14] to define the set of linear combinations of Mueller matrix elements that provide the largest predictors of material damage state when observed in a bi-static configuration. Looking at four classes of objects at 25 orientation configurations, we defined the following linear combinations of Mueller elements as the scene space,

$$
\underline{\underline{\mathbf{Y}}} = \begin{bmatrix}
-0.9204 & 0.3097 & 0.2378 \\
-0.0347 & 0.0410 & -0.2480 \\
-0.0010 & 0.0034 & -0.0136 \\
-0.0003 & 0.0007 & 0.0088 \\
-0.0318 & 0.0524 & -0.2356 \\
-0.2757 & -0.4730 & -0.4418 \\
-0.0010 & -0.0043 & -0.0050 \\
-0.0004 & 0.0033 & -0.0085 \\
0.0035 & -0.0039 & 0.0207 \\
0.0013 & -0.0043 & 0.0138 \\
0.2703 & 0.4860 & 0.3996 \\
-0.0019 & -0.0033 & -0.0220 \\
-0.0004 & 0.0008 & -0.0008 \\
0.0001 & 0.0023 & -0.0037 \\
0.0028 & 0.0017 & 0.0292 \\
0.0398 & 0.6630 & -0.6850
\end{bmatrix}.
\tag{1}
$$

The goal of each optimization was then to find the system configuration that produces the closest possible sensor space, while reducing the number of measurements made or channels created. For the case of c-pMMPs, we used Hagen's spectropolarimeter[4] as the overall architectural base for the optimization and then identified conditions under which a partial measurement is made. The decision to use that particular system was not fundamental to the discovered outcomes; the principles used there apply to any channeled system. However, because Hagen's system represents a set of single-domain modulation carriers, working with it proved more straightforward—there is no additional complexity of multiple-domain carrier splitting and enumeration. The overall principle of Hagen's system is introduction of four spectral carriers that create channels within the respective conjugate Fourier-domain, optical path difference (OPD), spaced accoringly to the thickness parameters of the birefringent plates as described by $\underline{\mathbf{d}}$. The candidate c-pMMP systems were then found by making superficial code adjustments that allowed for further loosening of the optimization constraints—a zero frequency was interpreted as a null-element. Because this modification would inadvertantly limit the number of reconstructable Mueller element, we adjusted the setup by introducing two additional zero-order retarders in PSA and PSG to provide the additional capacity to rotate the channel structure to obtain the best possible match between the scene space and the sensor space.[12,15] Figure 2 shows the system setup and the final pareto-surface of the optimization, while Fig. 3 shows results from two c-pMMPs: #4 is able to match sensor and scene spaces almost perfectly, while #1 has a class separation on the order of 40% of what a full system would produce. Although a disadvantage, c-pMMP #1 represents an efficient system that has nine channels and nine reconstructables. It removes two of the four

carriers, resulting in better noise resilience and bandwidth. The principles of the 9-c-pMMP are not limited to using Hagen's setup as the base—an equivalent exists when using Kudenov's setup as the base.[7] Figure 1 shows how the spatial-spatial channeled system can be devolved into a 9-c-pMMP of 1f.

(a) Hagen's configuration, $\underline{\mathbf{d}} = [1\ 2\ 5\ 10]$

(b) Rotated configuration, $\underline{\mathbf{d}}$ is variable

(c) Pareto-surface of optimal solutions
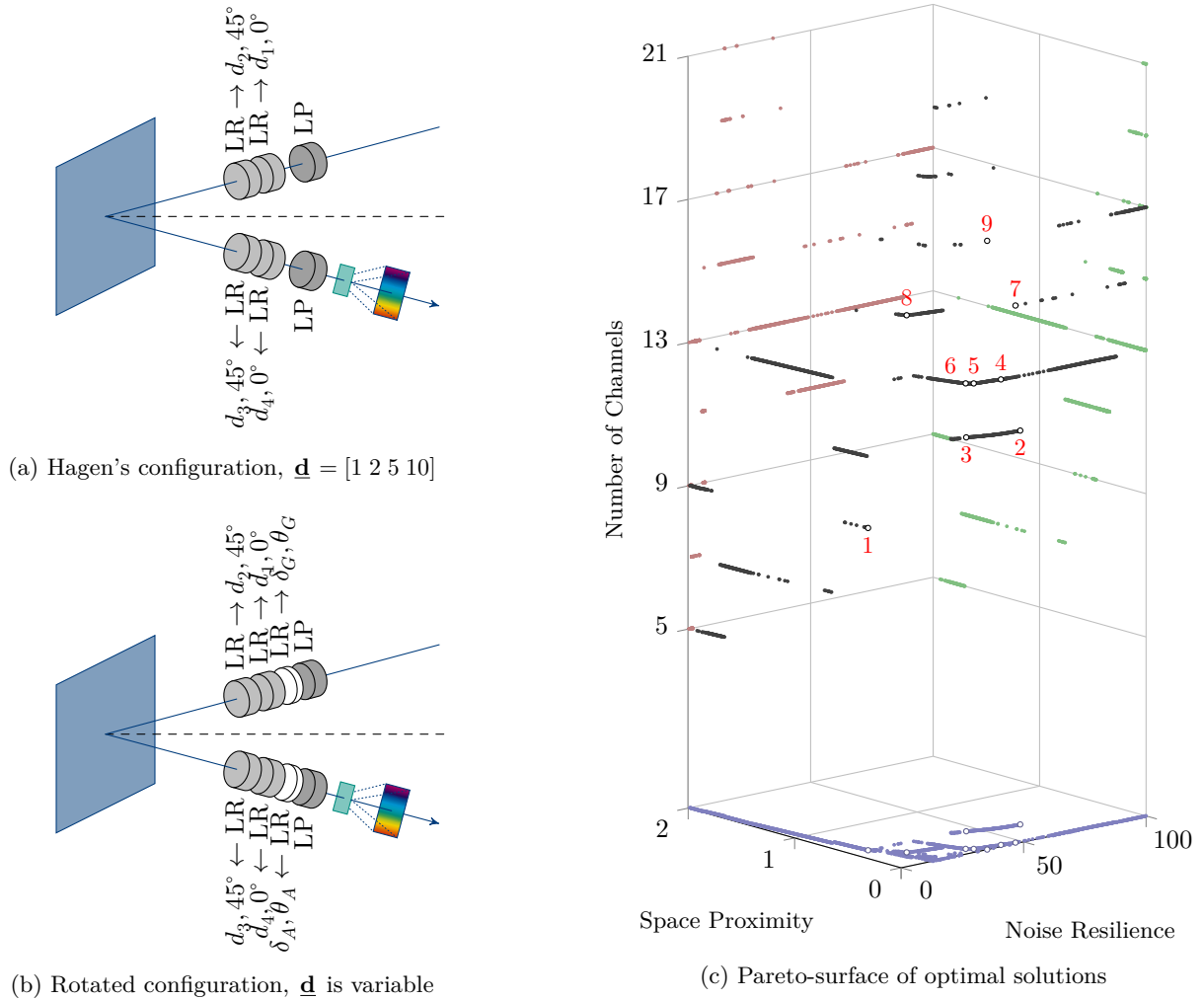
Figure 2: Adaptation of the system layout and the resulting solution space.

(a) c-pMMP #4, $N = R = 13$

(b) c-pMMP #1, $N = R = 9$
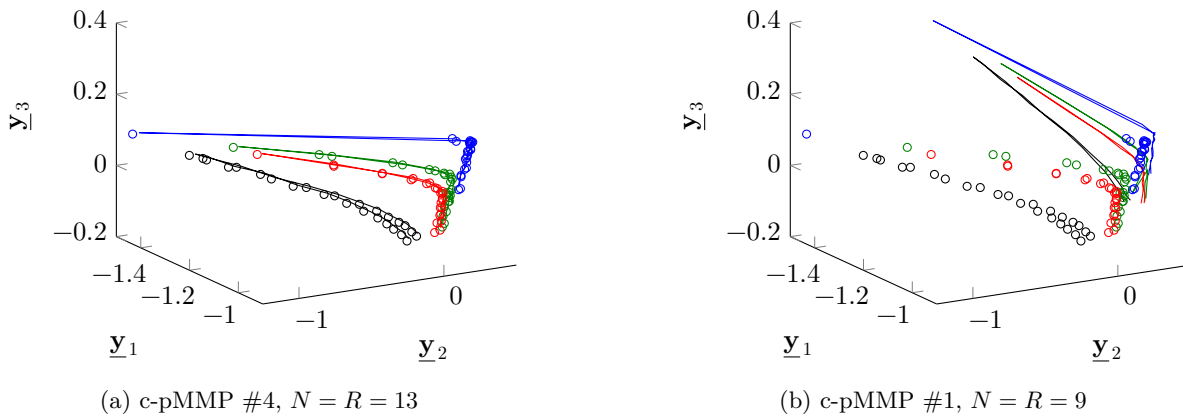
Figure 3: Space coverage afforded by different c-pMMP designs.

2. CHANNELED FORMALISM

A polarimetric measurement is a sum of products,

$$I\left(\vec{\vartheta}\right) = \sum_{i=0}^{3} \sum_{j=0}^{3} f_{a,i}\left(\vec{\vartheta}\right) m_{ij}\left(\vec{\vartheta}\right) f_{g,j}\left(\vec{\vartheta}\right), \tag{2}$$

where m_{ij} is the Mueller element content, while f_g and f_a are modulating functions that vary over the set of domains, $\vec{\vartheta}$. Channeled systems perform the same operation, but by constraining the modulation functions to a combination of M sinusoids,

$$f_{ij}\left(\vec{\vartheta}\right) = \prod_{m=1}^{M} {\textstyle{\cos \atop \sin}} \left(2\pi\xi_m x\right), \tag{3}$$

and selecting appropriate carrier frequencies, ξ_ms, we can shape a favorable channel structure within the Fourier domain of the measurement. To describe the channel structure, we analytically calculate the Fourier transform of those functions by forming two auxiliary matrices:

$$\underline{\underline{\mathbf{F}}}_M = \left[\begin{array}{cccc} \underline{\mathbf{f}}_1 & \underline{\mathbf{f}}_2 & \cdots & \underline{\mathbf{f}}_M \end{array}\right], \text{ where } f_{m,k} = \begin{cases} 0 & \text{if } \cos \\ 1 & \text{if } \sin \end{cases}, \tag{4}$$

$$\underline{\underline{\mathbf{O}}}_M = \left[\begin{array}{cccc} \underline{\mathbf{o}}_1 & \underline{\mathbf{o}}_2 & \cdots & \underline{\mathbf{o}}_M \end{array}\right], \text{ where } o_{m,\ell} = \begin{cases} -1 & \text{if } -\xi_i \\ +1 & \text{if } +\xi_i \end{cases}, \tag{5}$$

from which we calculate the Frequency Phase Matrix (FPM),

$$\underline{\underline{\mathbf{P}}}_M \equiv \frac{1}{2^M} \exp\left[\frac{-\mathrm{j}\pi}{2}\left(\underline{\underline{\mathbf{F}}}_M \underline{\underline{\mathbf{O}}}_M^{\mathrm{T}}\right)\right], \tag{6}$$

which can be seen in Fig. 4. Each row of the FPM represents the channel structure imposed on a Mueller element, as a consequence of the particular combination of functions and frequencies.
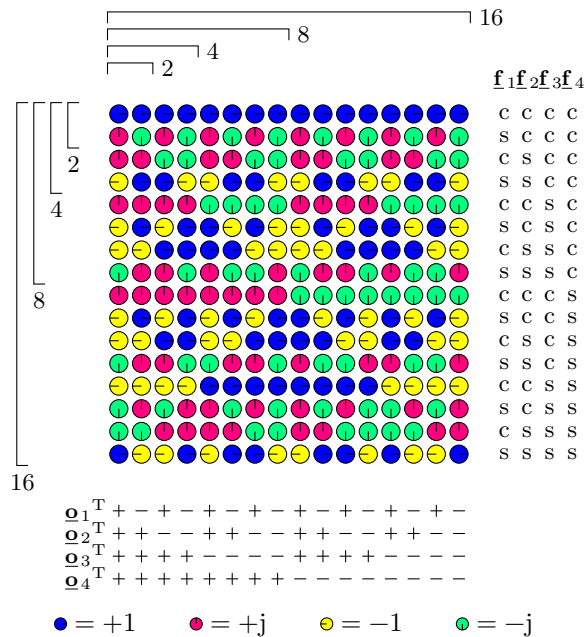
Figure 4: FPM for four sinusoid modulations. Although each row represents the applied modulation completely, it can reference potentially the same frequencies multiple times. For example, if $\xi_i = \xi_j$, the coefficients of $\delta(\xi - \xi_i + \xi_j)$ and $\delta(\xi + \xi_i - \xi_j)$ will interfere.

Each element's multiple-domain modulations can be described in a number of equivalent ways:

$$\underline{\mathbf{q}}_{\{\tau,\omega,\xi,\eta\};m_{ij}} = \underline{\mathbf{q}}_{\{\tau\};m_{ij}} \otimes \underline{\mathbf{q}}_{\{\omega\};m_{ij}} \otimes \underline{\mathbf{q}}_{\{\xi\};m_{ij}} \otimes \underline{\mathbf{q}}_{\{\eta\};m_{ij}}, \tag{7a}$$

$$= \mathrm{vec}\left(\underline{\mathbf{q}}_{\xi_{e_1};m_{ij}} * \underline{\mathbf{q}}_{\eta_{e_2};m_{ij}} * \underline{\mathbf{q}}_{\xi_{e_3};m_{ij}} * \underline{\mathbf{q}}_{\eta_{e_4};m_{ij}} \right), \tag{7b}$$

$$= \mathrm{vec}\left(\underline{\mathbf{q}}_{\{\tau,\omega,\xi,\eta\},g_i} * \underline{\mathbf{q}}_{\{\tau,\omega,\xi,\eta\},a_j} \right). \tag{7c}$$

The first method isolates modulations within each domain and treats them orthogonally with the Kronecker product. The second method recognizes that each carrier-inducing element has an associated modulation and combines them all with an M-dimensional convolution. Finally, the third method is a natural extension of the second method for having identified all of the modulations implied by the carrier-inducing elements within PSG and PSA first and then combining those in turn. Depending on how modulations are achieved, one way may be easier to implement than another. However, regardless of the approach selected, the same set of channel vectors for each Mueller element will result. Once derived, the 16 channel structures (one for each Mueller element) can be concatenated together into $\underline{\underline{\mathbf{Q}}}$,

$$\underline{\underline{\mathbf{Q}}} = \begin{bmatrix} \underline{\mathbf{q}}^{\mathrm{T}}_{\{\tau,\omega,\xi,\eta\};m_{00}} \\ \underline{\mathbf{q}}^{\mathrm{T}}_{\{\tau,\omega,\xi,\eta\};m_{01}} \\ \underline{\mathbf{q}}^{\mathrm{T}}_{\{\tau,\omega,\xi,\eta\};m_{02}} \\ \underline{\mathbf{q}}^{\mathrm{T}}_{\{\tau,\omega,\xi,\eta\};m_{03}} \\ \underline{\mathbf{q}}^{\mathrm{T}}_{\{\tau,\omega,\xi,\eta\};m_{10}} \\ \underline{\mathbf{q}}^{\mathrm{T}}_{\{\tau,\omega,\xi,\eta\};m_{11}} \\ \underline{\mathbf{q}}^{\mathrm{T}}_{\{\tau,\omega,\xi,\eta\};m_{12}} \\ \underline{\mathbf{q}}^{\mathrm{T}}_{\{\tau,\omega,\xi,\eta\};m_{13}} \\ \underline{\mathbf{q}}^{\mathrm{T}}_{\{\tau,\omega,\xi,\eta\};m_{20}} \\ \underline{\mathbf{q}}^{\mathrm{T}}_{\{\tau,\omega,\xi,\eta\};m_{21}} \\ \underline{\mathbf{q}}^{\mathrm{T}}_{\{\tau,\omega,\xi,\eta\};m_{22}} \\ \underline{\mathbf{q}}^{\mathrm{T}}_{\{\tau,\omega,\xi,\eta\};m_{23}} \\ \underline{\mathbf{q}}^{\mathrm{T}}_{\{\tau,\omega,\xi,\eta\};m_{30}} \\ \underline{\mathbf{q}}^{\mathrm{T}}_{\{\tau,\omega,\xi,\eta\};m_{31}} \\ \underline{\mathbf{q}}^{\mathrm{T}}_{\{\tau,\omega,\xi,\eta\};m_{32}} \\ \underline{\mathbf{q}}^{\mathrm{T}}_{\{\tau,\omega,\xi,\eta\};m_{33}} \end{bmatrix}^{\mathrm{T}}, \tag{8}$$

which serves as a mapping of the Fourier transform of the Mueller element information contained within the Mueller vector, $\underline{\mathbf{M}}$, into the measured Fourier channels, $\underline{\mathbf{C}}$, or

$$\mathcal{F}\{\underline{\mathbf{C}}\} = \underline{\underline{\mathbf{Q}}}\,\mathcal{F}\{\underline{\mathbf{M}}\}. \tag{9}$$

The measurement matrix is then inverted to produce the Mueller vector estimate,

$$\underline{\hat{\mathbf{M}}} = \mathcal{F}^{-1}\left\{ \underline{\underline{\mathbf{Q}}}^{+}\mathcal{F}\{\underline{\mathbf{C}}\} \right\}. \tag{10}$$

To solve the inverse problem, we use Singular Value Decomposition (SVD),[16] a choice which also readily reveals the system's performance. The measurement matrix can be decomposed as

$$\underline{\underline{\mathbf{Q}}} = \underline{\underline{\mathbf{U}}}_{\mathbf{Q}}\,\underline{\underline{\Sigma}}_{\mathbf{Q}}\,\underline{\underline{\mathbf{V}}}_{\mathbf{Q}}^{\dagger}, \tag{11}$$

where mathematically, $\underline{\underline{\mathbf{U}}}_{\mathbf{Q}}$ and $\underline{\underline{\mathbf{V}}}_{\mathbf{Q}}$ are $N_C \times R$ and 16×16 unitary orthogonal matrices containing the left and the right singular vectors, respectively, while matrix $\underline{\underline{\Sigma}}$ is an $R \times 16$ diagonal matrix containing singular values. N_C is the number of channels and R is the rank of $\underline{\underline{\mathbf{Q}}}$. The pseudo-inverse can then be written as:

$$\underline{\underline{\mathbf{Q}}}^{+} = \underline{\underline{\mathbf{V}}}_{\mathbf{Q}}\,\underline{\underline{\Sigma}}_{\mathbf{Q}}^{+}\,\underline{\underline{\mathbf{U}}}_{\mathbf{Q}}^{\dagger}. \tag{12}$$

3. 9-C-PMMP

The base channeled polarimeter from our prior work[13] can be described with the following modulation functions:

$$\underline{\mathbf{f}}_{\mathbf{G}} = \begin{bmatrix} 1 \\ \cos(2\pi\vartheta_1\tilde{\vartheta}_1) \\ \sin(2\pi\vartheta_1\tilde{\vartheta}_1)\sin(2\pi\vartheta_2\tilde{\vartheta}_2) \\ \sin(2\pi\vartheta_1\tilde{\vartheta}_1)\cos(2\pi\vartheta_2\tilde{\vartheta}_2) \end{bmatrix}, \tag{13a}$$

$$\underline{\mathbf{f}}_{\mathbf{A}} = \begin{bmatrix} 1 \\ \cos(2\pi\vartheta_4\tilde{\vartheta}_4) \\ \sin(2\pi\vartheta_3\tilde{\vartheta}_3)\sin(2\pi\vartheta_4\tilde{\vartheta}_4) \\ \cos(2\pi\vartheta_3\tilde{\vartheta}_3)\sin(2\pi\vartheta_4\tilde{\vartheta}_4) \end{bmatrix}, \tag{13b}$$

where ϑ_is are the domains and $\tilde{\vartheta}_i$s are the carrier frequencies within the respective conjugate domains. By removing two elements, we arrive at the default 9-c-pMMP design, which can be described with the following modulation functions:

$$\underline{\mathbf{f}}_{\mathbf{G}} = \begin{bmatrix} 1 \\ \cos(2\pi\vartheta_1\tilde{\vartheta}_1) \\ \sin(2\pi\vartheta_1\tilde{\vartheta}_1) \\ 0 \end{bmatrix}, \tag{14a}$$

$$\underline{\mathbf{f}}_{\mathbf{A}} = \begin{bmatrix} 1 \\ \cos(2\pi\vartheta_4\tilde{\vartheta}_4) \\ \sin(2\pi\vartheta_4\tilde{\vartheta}_4) \\ 0 \end{bmatrix}. \tag{14b}$$

The fact that $a_3 = g_3 = 0$ means that the default configuration is insensitive to the fourth row and the fourth column of the Mueller matrix. By adding the two extra zero-order linear retarders: one within PSA, one within PSG; we avoid inducing any additional carriers while allowing us to change the set of linear combinations of Mueller elements that we are sensitive to. Since the Mueller matrix for a linear retarder is a unitary matrix, we can more accurately call this a rotated configuration. The reconstructables rotation is achieved by varying the four parameters, $\{\delta_A, \delta_G, \theta_A, \theta_G\}$. Within the original c-pMMP treatment, they were additional optimization parameters used in sensor/scene space alignment

The first 9-c-pMMP was discovered within the one-dimensional spectral modulation based off of Hagen's design,[4] when we removed two elements and set $3d_1 = d_4$, we arrive at the 9×1 channel structure shown in Fig. 7a. However, a mathematically equivalent design exists within the two-dimensional spatial modulation based off of Kudenov's design.[7] That design involves polarization gratings and focusing optics in-between to create a different carrier frequencies. Again, by removing two of the four carrier-inducing elements, we arrive at the 3×3 channel structure shown in Fig. 7b. The steps taken to produce these two systems are summarized in Figs. 5 and 6. The default configuration of the 9-c-pMMP has $\delta_A = \delta_G = \theta_A = \theta_G = 0$, which corresponds to following sensor space:

$$\underline{\underline{\mathbf{V}}}'_{\vec{0}} = \begin{bmatrix} \mathbf{v}_{\vec{0},1} & \mathbf{v}_{\vec{0},2} & \cdots & \mathbf{v}_{\vec{0},9} \end{bmatrix} = \begin{bmatrix} \mathbb{I}_{3\times3} & \mathbb{0}_{3\times3} & \mathbb{0}_{3\times3} \\ \mathbb{0}_{1\times3} & \mathbb{0}_{1\times3} & \mathbb{0}_{1\times3} \\ \mathbb{0}_{3\times3} & \mathbb{I}_{3\times3} & \mathbb{0}_{3\times3} \\ \mathbb{0}_{1\times3} & \mathbb{0}_{1\times3} & \mathbb{0}_{1\times3} \\ \mathbb{0}_{3\times3} & \mathbb{0}_{3\times3} & \mathbb{I}_{3\times3} \\ \mathbb{0}_{5\times3} & \mathbb{0}_{5\times3} & \mathbb{0}_{5\times3} \end{bmatrix}. \tag{15}$$

By calculating the reconstructable matrix, we see a clear delineation of sensitivity to the linear-linear transformations of the Mueller matrix space,

$$\underline{\underline{\mathbf{B}}}_{\vec{0}} = \mathrm{mat}\left(\mathrm{diag}\left(\underline{\underline{\mathbf{V}}}'_{\vec{0}}\underline{\underline{\mathbf{V}}}'^{\mathrm{T}}_{\vec{0}}\right)\right) = \begin{bmatrix} 1 \\ 1 \\ 1 \\ 0 \end{bmatrix}\begin{bmatrix} 1 \\ 1 \\ 1 \\ 0 \end{bmatrix}^{\mathrm{T}} = \begin{bmatrix} 1 & 1 & 1 & 0 \\ 1 & 1 & 1 & 0 \\ 1 & 1 & 1 & 0 \\ 0 & 0 & 0 & 0 \end{bmatrix}. \tag{16}$$

(a) Four carriers (b) Two carriers (c) Two carriers and rotation
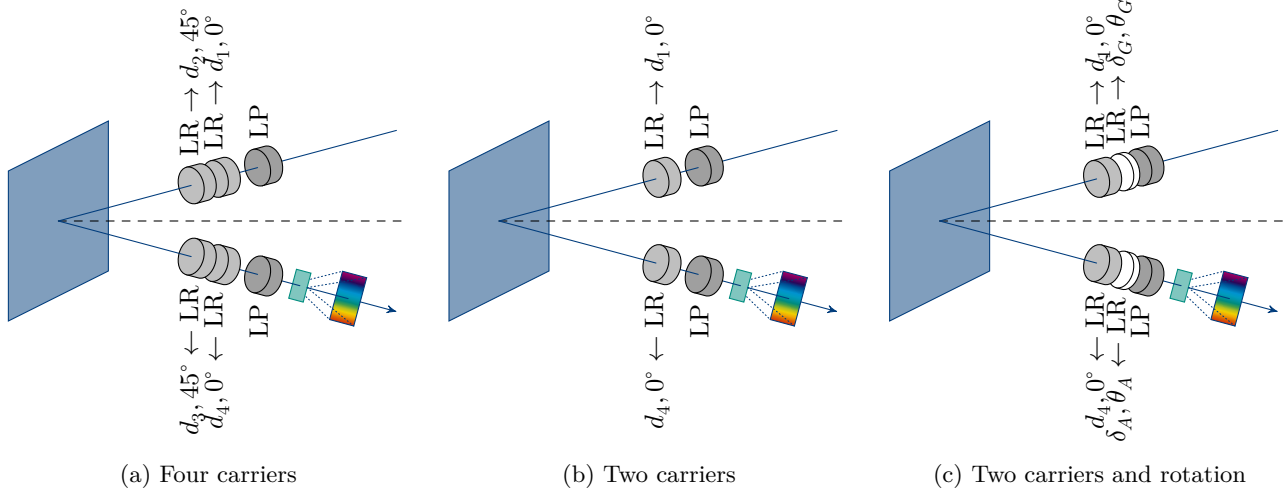
Figure 5: Spectrally modulated channeled polarimeter

(a) Four carriers (b) Two carriers (c) Two carriers and rotation
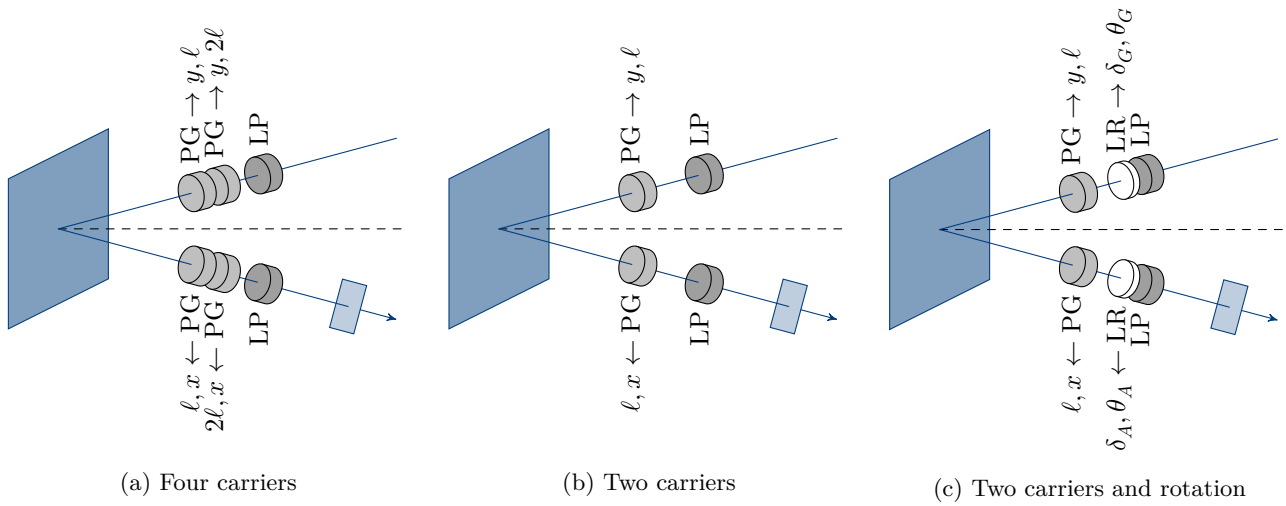
Figure 6: Spatially modulated channeled polarimeter

(a) Spectrally channeled 9-c-pMMP (b) Spatially channeled 9-c-pMMP
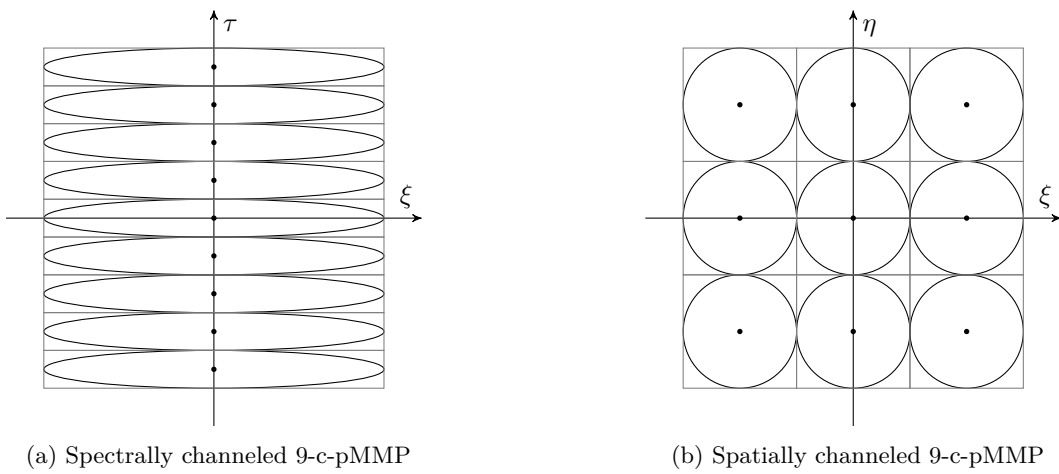
Figure 7: Channel structures and allocated bandwidth of the two 9-c-pMMPs.

In order to track variance distribution with a bit more clarity, we introduce notation to make the distinction of equally-weighted variance (EWV) for a variable number of reconstructables, EWV_R, where R is the rank of the matrix. An optimal channeled full single-snapshot polarimeter has $R = 16$, implying sensitivity to the entire Mueller matrix. The summary metric of $\text{EWV}_{16} = 121$ is borne out of the familiar set of variances:[9]

$$\text{EWV}_{16} = \sum \sum \begin{bmatrix} 1 \\ 2 \\ 4 \\ 4 \end{bmatrix} \begin{bmatrix} 1 \\ 2 \\ 4 \\ 4 \end{bmatrix}^{\text{T}} = \sum \sum \begin{bmatrix} 1 & 2 & 4 & 4 \\ 2 & 4 & 8 & 8 \\ 4 & 8 & 16 & 16 \\ 4 & 8 & 16 & 16 \end{bmatrix} = 121. \tag{17}$$

However, for the 9-c-pMMP, we have one fewer modulations in both PSA and PSG, resulting in $R = 9$ and the following set of variances:

$$\text{EWV}_9 = \sum \sum \begin{bmatrix} 1 \\ 2 \\ 2 \\ \varnothing \end{bmatrix} \begin{bmatrix} 1 \\ 2 \\ 2 \\ \varnothing \end{bmatrix}^{\text{T}} = \sum \sum \begin{bmatrix} 1 & 2 & 2 & \varnothing \\ 2 & 4 & 4 & \varnothing \\ 2 & 4 & 4 & \varnothing \\ \varnothing & \varnothing & \varnothing & \varnothing \end{bmatrix} = 25. \tag{18}$$

An equally apt demonstration of the principle behind this result can be seen in Fig. 2c, where the nine-channeled system shows a better noise resilience when compared to its "bigger siblings". Thus, this design represents a clear trade-off—we can measure fewer elements with higher accuracy.

For the rotated configuration, we can show that the following expression transforms a default vector into a rotated vector of the sensor space:

$$\underline{\mathbf{v}}_{\vec{\xi},i} = \text{vec}\left(\underline{\underline{\mathbf{M}}}_{\text{LR}}(\delta_G, \theta_G) \, \text{mat}(\underline{\mathbf{v}}_{\vec{0},i}) \underline{\underline{\mathbf{M}}}_{\text{LR}}(\delta_A, \theta_A)\right), \tag{19}$$

where vec is used to vectorize a 4×4 matrix in row-by-row fashion into a 16×1 vector, while mat is used to consistently matricize a 16×1 vector into a 4×4 matrix. The rotated configuration's sensor space is then simply a concatenation of all nine rotated vectors:

$$\underline{\underline{\mathbf{V}}}_{\vec{\xi}}' = \begin{bmatrix} \underline{\mathbf{v}}_{\vec{\xi},1} & \underline{\mathbf{v}}_{\vec{\xi},2} & \cdots & \underline{\mathbf{v}}_{\vec{\xi},9} \end{bmatrix}, \tag{20}$$

which can be shown to produce the following reconstructables matrix:

$$\underline{\underline{\mathbf{B}}}_{\vec{\xi}} = \begin{bmatrix} 1 \\ 1 - \sin^2 2\theta_A \sin^2 \delta_A \\ 1 - \cos^2 2\theta_A \sin^2 \delta_A \\ \sin^2 \delta_A \end{bmatrix} \begin{bmatrix} 1 \\ 1 - \sin^2 2\theta_G \sin^2 \delta_G \\ 1 - \cos^2 2\theta_G \sin^2 \delta_G \\ \sin^2 \delta_G \end{bmatrix}^{\text{T}}. \tag{21}$$

Because $(1 - \sin^2 2\theta \sin^2 \delta) + (1 - \cos^2 2\theta \sin^2 \delta) + (\sin^2 \delta) = 2$, a rotated 9-c-pMMP maintains access to $2/3$ rank-units within the polarizance and diattenuation vectors of the Mueller matrix, as well as $4/9$ rank-units within the 3×3 rotation block as obtained with the Kronecker product. It is important to note that just like with full systems, this rotation does not change EWV_R; the same variances from Eq. 18 will be true for some calculable—but not necessarily obvious—linear combinations within the Mueller matrix space.

We performed a similar rotation in the original generalized channeled polarimetry treatment,[9] where we looked at the possibility of performing multiple snapshots, with each one having a different set of parameters. The analysis was performed on a Kudenov-like spatial configuration of Fig. 6, and the results can be seen in Table 1. Note that the number of channels within PSA and PSG channel structures is dictated by the values of d_i; for example, $1/1/1/1$ in $y/y/x/x$ creates a 5×5 channel structure, while $2/1/1/2$ in $y/y/x/x$ creates a 7×7 channel structure. From the numbers, it is evident that you have to create a 7×7 channel structure in order to have an optimal single-snapshot channeled system with $\text{EWV} = 121$. However, if the temporal constraints are loose enough to get away with multiple snapshots, then the EWV of 5×5 and 5×7 systems become more competitive as the number of snapshots increases. This can be understood to mean that an increasing number

of diverse snapshots enables previously-unavailable channel structures that are as-a-whole easier to unmix. In order to tackle these channel structures, we simply concatenate N individual snapshots as shown in Figure 8,

$$\underline{\underline{\mathbf{Q}}}_{\text{total}} = \begin{bmatrix} \underline{\underline{\mathbf{Q}}}_1^{\text{T}} & \underline{\underline{\mathbf{Q}}}_2^{\text{T}} & \cdots & \underline{\underline{\mathbf{Q}}}_N^{\text{T}} \end{bmatrix}^{\text{T}}. \tag{22}$$
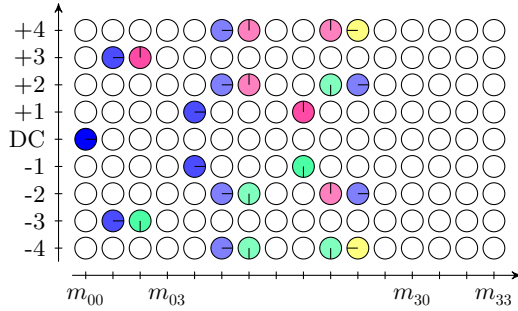
(a) 1-snapshot default 9-c-pMMP
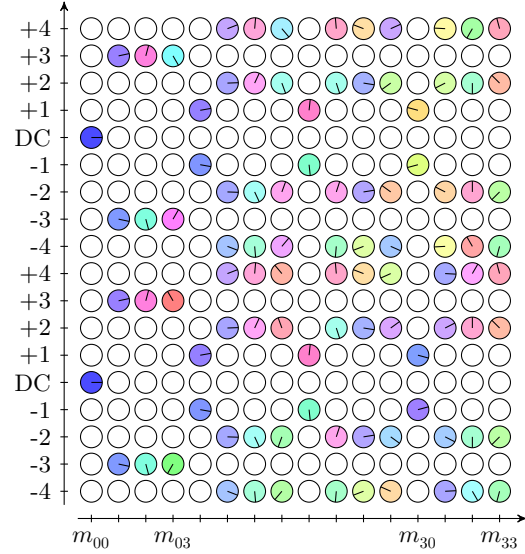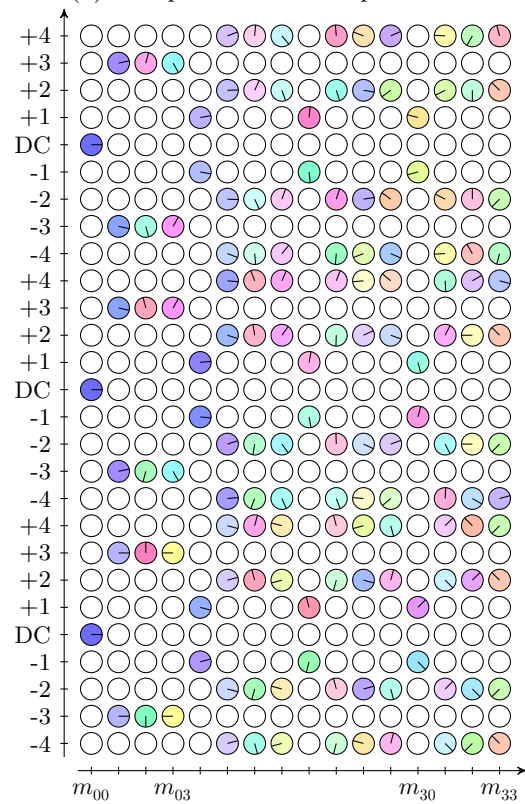
(b) 1-snapshot rotated 9-c-pMMP

(c) 1-snapshot rotated 9-c-pMMP

(d) 2-snapshot rotated 9-c-pMMP

(e) 3-snapshot rotated 9-c-pMMP
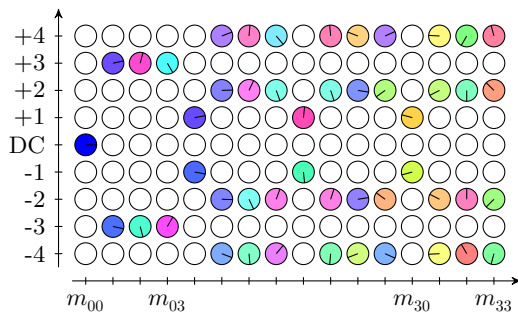
Figure 8: $\underline{\underline{\mathbf{Q}}}$ for different number of snapshots with 9-c-pMMP

This reduction of unmixing complexity as a result of increased number of snapshots also exists for multi-snapshot 9-c-pMMPs. In fact, if temporal bandwidth is less critical than spatial bandwidth and going to three snapshots is acceptable, then the 9-c-pMMP enables a very interesting option. As can be seen from Table 2, three partial snapshots perform only about 7% worse in noise resilience, while allowing the spatial bandwidth increase to 233% of the 7×7 system in both x and y, which corresponds to each channel containing 544% the number of frequencies. Figure 9 summarizes the spatial bandwidth advantage of the multi-snapshot 9-c-pMMP. Also included in that comparison is a two-snapshot 5×5 channel system, which is only competitive in a multi-snapshot configuration, while providing a highly non-optimal $\text{EWV}_{16} = 441$ in single-snapshot mode. Overall, this analysis introduces a clear trade-off between spatial and temporal bandwidths—by modulating in both, we can tailor the resolution of our reconstructed data for the set of conditions the given application entails.[17]

Table 1: EWV of multi-snapshot full channeled polarimeters. The row and column entries refer to d_1/d_2 and d_3/d_4 parameters, respectively. The symmetry of PSA/PSG calculations is evident.

	1/1	2/1	1/2	2/2		1/1	2/1	1/2	2/2
1/1	441.0	171.7	214.9	151.0	1/1	60.00	53.50	53.60	53.60
2/1	171.7	121.0	147.7	147.7	2/1	53.50	53.57	54.28	53.50
1/2	214.9	147.7	133.0	214.9	1/2	53.60	54.28	56.22	59.08
2/2	151.0	147.7	214.9	441.0	2/2	53.60	53.50	59.08	60.00
	(a) 1-Snapshot Full Design					(b) 2-Snapshot Full Design			
	1/1	2/1	1/2	2/2		1/1	2/1	1/2	2/2
1/1	36.26	35.50	35.32	35.00	1/1	25.33	25.48	25.52	25.65
2/1	35.50	34.00	34.50	34.77	2/1	25.48	25.22	25.61	25.61
1/2	35.32	34.50	35.20	35.95	1/2	25.52	25.61	25.78	26.16
2/2	35.00	34.77	35.95	36.49	2/2	25.65	25.61	26.16	25.94
	(c) 3-Snapshot Full Design					(d) 4-Snapshot Full Design			

Table 2: Multi-snapshot 9-c-pMMP designs and EWV performance.

N	R	δ_G	δ_A	θ_G	θ_A	EWV_R
1	9	–	–	–	–	25.00
2	14	$\cos^{-1}(1/\sqrt{3})$	$\cos^{-1}(1/\sqrt{3})$	$\{37.5°, 82.5°\}$	$\{15°, 60°\}$	39.60
3	16	$\cos^{-1}(1/\sqrt{3})$	$\cos^{-1}(1/\sqrt{3})$	$\{37.5°, 97.5°, 157.5°\}$	$\{15°, 75°, 135°\}$	36.33
4	16	$\cos^{-1}(1/\sqrt{3})$	$\cos^{-1}(1/\sqrt{3})$	$\{37.5°, 82.5°, 127.5°, 172.5°\}$	$\{15°, 60°, 105°, 150°\}$	26.65

(a) 49 channels — 100% bandwidth good full performance at 1 snapshots

(b) 25 channels — 140% bandwidth good full performance at 2 snapshots

(c) 9 channels — 233% bandwidth good full performance at 3 snapshots
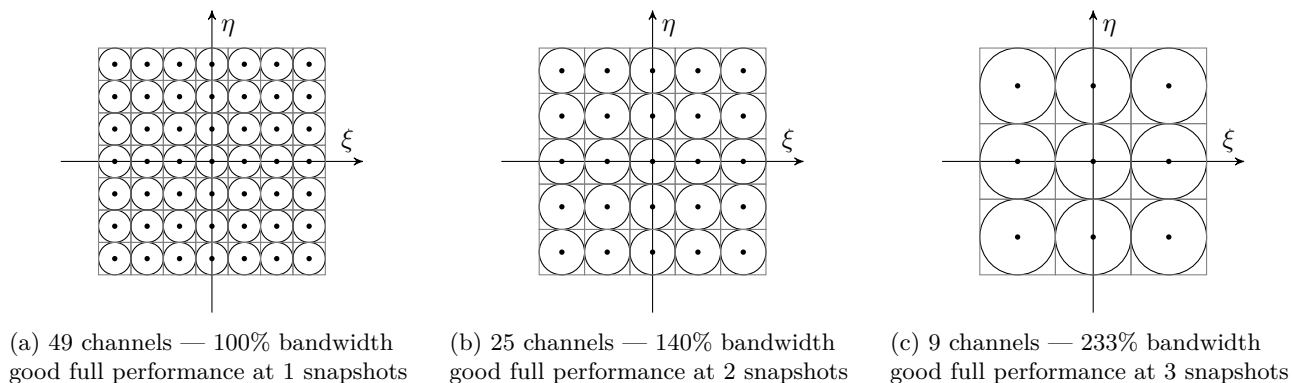
Figure 9: Channel structures and bandwidth of multi-snapshot systems

4. CONCLUSION

In this extension of the c-pMMP analysis, we have taken a first detailed look at the implications of the 9-c-pMMP. This system provides a unique set of trade-offs; by discarding two out of the four carrier-inducing polarization elements, the system is simplified in a variety of ways. For the spatially modulated 9-c-pMMP, we can use a single carrier in each of the two spatial domains, thereby eliminating the need for careful alignment of various focusing optics to match the intended interference. For the spectrally modulated 9-c-pMMP, the difficulty of assembly is also lessened through not having to worry about the thickness mismatch—as long as one of the frequencies is equal to or greater than three times the other, channels will not incur any extra interference. Furthermore, the reduced number of modulations enable channels with more bandwidth, and of better noise resilience as well.

The biggest drawback to a 9-c-pMMP system is that its architecture might not always be adjustable enough to measure the desired set of Mueller elements in a single-snapshot. However, in the case that some temporal bandwidth can be given up, a 9-c-pMMP can be used in a multi-snapshot configuration. And if we look at an optimal 7×7 spatially-modulated channeled polarimeter as one extreme, and a conventional Mueller matrix taking 16 snapshots as another, the three-snapshot hybrid modulation presents a great alternative. Instead of giving up a factor of 49 in spatial bandwidth or a factor of 16 in temporal bandwidth, we can spread out the loss of resolution and give up a factor of 9 in spatial bandwidth and a factor of 3 in temporal bandwidth.

Though the results in Table 2 indicate that there exist two- and three-snapshot systems that result in rank 14 and 16 reconstructions, these ranks are not a guarantee. Depending on how you structure the parameters of the additional linear retarders will determine whether you are sensing the Mueller space efficiently. In order to assess how the individual snapshots combine in the multi-snapshot mode, we need to apply structured decomposition techniques[12] to the 9-c-pMMP architecture. We intend to publish on the outcome of that analysis later—it is expected that the constraints that exist within the two-snapshot mode will prove to be the most interesting. Finally, we plan to build this system in order to confirm its performance and the effects of misalignment.

ACKNOWLEDGMENTS

REFERENCES

[1] K. Oka and T. Kato, "Spectroscopic polarimetry with a channeled spectrum," Opt. Lett. **24**, 1475–1477 (1999).

[2] K. Oka and T. Kaneko, "Compact complete imaging polarimeter using birefringent wedge prisms," Opt. Express **11**, 1510–1519 (2003).

[3] H. Okabe, M. Hayakawa, H. Naito, A. Taniguchi, and K. Oka, "Spectroscopic polarimetry using channeled spectroscopic polarization state generator (CSPSG)," Opt. Express **15**, 3093–3109 (2007).

[4] N. Hagen, K. Oka, and E. L. Dereniak, "Snapshot Mueller matrix spectropolarimeter," Opt. Lett. **32**, 2100–2102 (2007).

[5] M. Dubreuil, S. Rivet, B. L. Jeune, and J. Cariou, "Snapshot Mueller matrix polarimeter by wavelength polarization coding," Opt. Express **15**, 13660–13668 (2007).

[6] P. Lemaillet, S. Rivet, and B. L. Jeune, "Optimization of a snapshot Mueller matrix polarimeter," Opt. Lett. **33**, 144–146 (2008).

[7] M. W. Kudenov, M. J. Escuti, N. Hagen, E. L. Dereniak, and K. Oka, "Snapshot imaging Mueller matrix polarimeter using polarization gratings," Opt. Lett. **37**, 1367–1369 (2012).

[8] A. S. Alenin and J. S. Tyo, "Task-specific snapshot Mueller matrix channeled spectropolarimeter optimization," Proc. SPIE **8364**, 836402 (2012).

[9] A. S. Alenin and J. S. Tyo, "Generalized channeled polarimetry," J. Opt. Soc. Am. A **31**, 1013–1022 (2014).

[10] A. S. Alenin, I. J. Vaughn, and J. S. Tyo, "Optimal bandwidth micropolarizer arrays," Opt. Lett. **42**, 458–461 (2017).

[11] I. J. Vaughn, A. S. Alenin, and J. S. Tyo, "Focal plane filter array engineering I: rectangular lattices," Opt. Express **25**, 11954–11968 (2017).

[12] A. S. Alenin and J. S. Tyo, "Structured decomposition design of partial Mueller matrix polarimeters," J. Opt. Soc. Am. A **32**, 1302–1312 (2015).

[13] A. S. Alenin and J. S. Tyo, "Design of channeled partial mueller matrix polarimeters," J. Opt. Soc. Am. A **33**, 1060–1070 (2016).

[14] B. G. Hoover and J. S. Tyo, "Polarization components analysis for invariant discrimination," Appl. Opt. **46**, 8364–8373 (2007).

[15] J. S. Tyo, Z. Wang, S. J. Johnson, and B. G. Hoover, "Design and optimization of partial Mueller matrix polarimeters," Appl. Opt. **49**, 2326–2333 (2010).

[16] G. H. Golub and C. F. van Loan, *Matrix Computations* (Johns Hopkins University Press, Baltimore, MD, 1983), chap. 2, pp. 11–29.

[17] J. S. Tyo and A. S. Alenin, "Bandwidth and information in the design and analysis of polarimeters," Proc. SPIE **9613**, 96130O (2015).